energies

MDPI

Article

Geospatial Forecasting of Electric Energy in Distribution Systems Using Segmentation and Machine Learning with Convolutional Methods

Héctor Chávez [1,*] and Yuri Molina [2]

[1] Faculty of Electrical and Electronic Engineering, National University of Engineering, Lima 15333, Peru
[2] Department of Electrical Engineering, Federal University of Paraíba, João Pessoa 58051-900, PB, Brazil; molina.rodriguez@cear.ufpb.br
* Correspondence: hector.chavez.a@uni.pe

Abstract: This paper proposes an innovative methodology for geospatial forecasting of electrical demand across various consumption segments and scales, integrating machine learning and discrete convolution within the framework of global system projections. The study was conducted in two phases: first, machine learning techniques were utilized to classify and determine the relative growth of segments with similar consumption patterns. In the second phase, convolution methods were employed to produce accurate spatial forecasts by incorporating the influence of neighboring areas through a "core matrix" and accounting for geographical constraints in regions with and without consumption. The proposed approach enhances the precision of spatial forecasts, making it suitable for large-scale distribution systems and implementable within short timeframes. The proposed method was validated using data from a Peruvian distribution system serving over one million users, employing 204 historical records and analyzing three georeferenced consumption segments at scales of 1:10,000, 1:1000, and 1:100. The results demonstrate its effectiveness in forecasting across different time horizons, thereby contributing to improved planning of electrical infrastructure.

Keywords: geospatial forecasting; discrete convolution; distribution system; segments; machine learning

Received: 7 December 2024
Revised: 13 January 2025
Accepted: 15 January 2025
Published: 19 January 2025

Citation: Chávez, H.; Molina, Y. Geospatial Forecasting of Electric Energy in Distribution Systems Using Segmentation and Machine Learning with Convolutional Methods. *Energies* **2025**, *18*, 424. https://doi.org/10.3390/en18020424

1. Introduction

The forecast of electrical demand is a crucial input in the planning of the electric industry, playing a significant role in the decision-making process of market agents, and is closely linked to economic, social, and environmental development [1,2]. It is essential for sustainability to optimize the use of energy resources aligned with renewable energy sources and the expansion of infrastructure over short, medium, and long-term horizons, while ensuring a stable supply of electricity and reducing carbon emissions [3,4]. This requires accurate predictions of demand, both in terms of magnitude and geographic locations, over different periods of the planning horizon.

Electric distribution companies are responsible for acknowledging their customers' needs and supplying energy efficiently while maintaining the electrical grid at an acceptable level of quality and reliability. These networks exhibit a high degree of variation in topology and are continuously expanding due to urban growth and the expansion of electrical service coverage areas [5,6].

Methods for projecting electrical demand are studied in terms of energy (kWh) and power (kW), considering short-, medium-, and long-term time horizons to meet the operational, planning, and other needs within electrical systems. These methods employ statistical techniques, artificial intelligence, and spatial micro-area analysis. Statistical methods explore models such as regression, multiple regression, exponential smoothing, iterative reweighted least squares, adaptive load forecasting, stochastic time series (autoregressive), ARMA, ARIMA, SARIMA, and Prophet models. On the other hand, artificial intelligence methods investigate neural networks, support vector machines, genetic algorithms, machine learning, wavelet neural networks, fuzzy logic methods, and expert systems [7–12]. Most methods focus on projections for the serviced area, assuming uniform growth across the region; however, in practice, growth is heterogeneous at different levels of granularity, and over the years new areas become serviced.

Various methodologies have been proposed for spatial prediction in electrical load forecasting. One notable method, introduced by [13], integrates current trends, a clustering algorithm, and a Geographic Information System (GIS) to perform spatial load forecasting. This approach utilizes fuzzy reasoning and fuzzy clustering algorithms to generate spatial load forecasts.

In the work of [14], a fuzzy inference system based on adaptive networks is applied to predict electrical loads across four major regions of Taiwan. Another significant contribution, presented in [15], employs cellular automata—a discrete-time model composed of cells that evolve according to predefined rules. This model emphasizes the significance of developed and redeveloped areas in spatial load forecasts. By leveraging data mining techniques, classification rules are extracted from a dataset with a spatial resolution of 0.5 km^2. The cellular automata approach assumes continuous load growth, where growth progresses incrementally, and undeveloped areas become developed when surrounded by at least three developed neighbors. This methodology builds on earlier research by the same group [16,17].

The dynamics of urban areas were analyzed using a multi-agent system in [18], focusing on the distribution of electrical loads across city subzones. This system incorporates static, mobile, and proactive agents, where mobile agents navigate the city, redistributing loads along their paths, and proactive agents represent new, non-natural loads introduced into the system. A spatial load forecasting method based on cluster analysis was proposed in [19], grouping cells by evaluating their results and relative prediction errors from multiple forecasting models. To predict energy consumption in multi-family residential buildings, support vector regression was employed in [20], leveraging on-site measurements for model development. Load monitoring for operational purposes was addressed in [21]. Furthermore, knowledge discovery in databases was utilized in [22] to extract preferential scores for land use changes in spatial load forecasting, while rough set theory was applied in [23]. Aerial imagery was also integrated into spatial load forecasting in [24] to enhance accuracy.

Spatiotemporal forecasting of energy demand plays a pivotal role in conducting detailed analyses in micro-areas and facilitating the efficient development of the electrical grid over various time horizons. This procedure enables a tailored adaptation to customer requirements while supporting strategic planning for future electrification zones. The availability of accurate geolocated demand data, both current and projected, is indispensable, particularly when addressing specific constraints such as capacity saturation and land use limitations. Forecasting at the micro-area level, while ensuring consistent geographical boundaries, provides a granular and precise representation of spatial consumption patterns. By leveraging spatial information, it becomes possible to achieve more accurate data aggregation, thereby minimizing distortions in system-wide demand forecasts.

The integration of machine learning and convolution methods applied to large-scale geospatial forecasting of electrical energy yields efficient results for use in the planning of medium- and long-term electrical distribution systems. Its computational implementation is highly effective for processing large volumes of data. The proposed algorithm facilitates the incorporation of the additive effects of major consumption centers in their surrounding areas through a "2N − 1" order kernel matrix. It also incorporates relative growths, geographic constraints, and saturation of consumption (S-curve), while aligning with the global forecast.

The proposed method for addressing the challenge of geospatial forecasting of electric energy in distribution systems offers several significant contributions:

- **Integration of machine learning and convolution techniques:** this study demonstrates the effectiveness of integrating machine learning algorithms with convolution methods for processing large datasets and conducting large-scale geospatial energy demand forecasts. The approach not only aligns with global forecasting results but also facilitates the identification and planning of new electrification areas, optimizing the management of electric distribution networks.
- **Segmentation of the distribution service area:** the proposed segmentation method divides the service area into grids, enabling precise identification of critical network components for analysis. This scalable approach adapts to the requirements of both sub-transmission and distribution systems. The phased segmentation model enhances network analysis, supporting more efficient and detailed system management.
- **Adaptability of geospatial analysis:** the geospatial analysis framework is adaptable to various global growth scenarios, integrating economic, social, and demographic factors for high accuracy. It allows spatial representation of optimistic and pessimistic growth projections over medium- and long-term horizons, adding strategic value to infrastructure planning and improving responsiveness to diverse demand scenarios.
- **Geospatial forecasting of energy demand:** accurate forecasting of medium- and long-term energy demand provides critical insights for planning the expansion of distribution and sub-transmission networks. This includes addressing areas without electrical coverage and those requiring electrification due to urban growth. The results support the development of new forecasting methods tailored to the characteristics of specific network components, improving overall energy planning strategies.
- **Enhancements to the regulatory and methodological framework:** the proposed methodology advances the regulatory framework for planning electrical transmission and distribution systems over short-, medium-, and long-term horizons. It introduces a systematic approach that electrical distribution companies can implement to enhance the precision and effectiveness of their expansion plans, contributing to both current practices and future procedural developments.

The structure of this work is organized as follows. Section 2 presents the theoretical foundation and introduces the key concepts necessary for understanding the paper. Section 3 describes the proposed method, detailing the step-by-step procedure and including a simplified example to enhance comprehension. Section 4 validates the methodology through its application to a real-world case study involving the "Luz del Sur" distribution system in Lima, Peru. Finally, Section 5 concludes the work by summarizing the main findings and discussing their implications.

2. Background Work

Developing prediction models for small areas effectively requires a focused analysis on specific elements of the electrical network, such as power substations, feeders, or distribution substations. These elements are analyzed based on the regions they serve, as illustrated

in Figure 1a for power substations [25]. However, this approach faces significant challenges due to the intricate geometries of the resulting areas and their temporal variability, which arise from the dynamic evolution of the electrical grid.

An alternative approach involves using square cells overlaid on a grid map, as depicted in Figure 1b. This method is readily implemented using databases or matrix arrays, with cell sizes adaptable to the scale of the network element under study. For instance, larger cells are suited for transmission facilities, while smaller cells are preferable for distribution facilities.

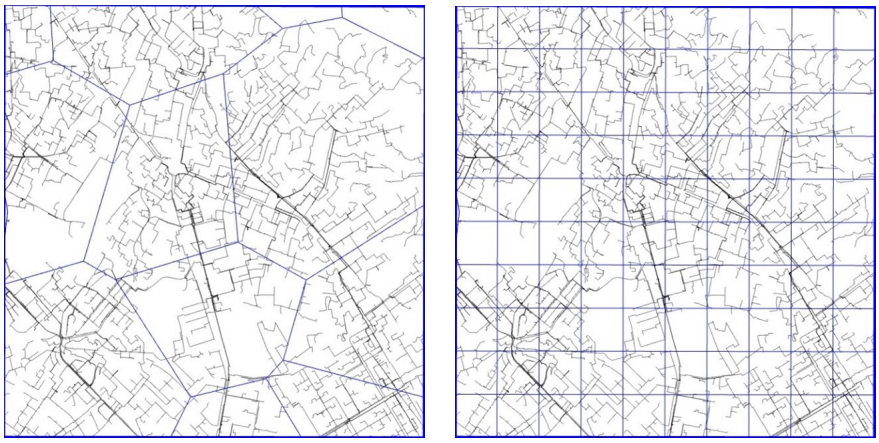

(**a**) (**b**)

Figure 1. Overview of network development. (**a**): Area of power substations and medium voltage network development; (**b**): medium voltage network development and grid mapping.

For geospatial forecasting, it is crucial to account for various factors, including the physical description of the electrical network, historical records of georeferenced customer consumption, and geographic data such as streets, mountains, lakes, rivers, roads, and archaeological sites, among others [26]. Additionally, global forecast results at the total system level must be considered. These factors can be effectively addressed by incorporating machine learning methods and convolution techniques, enabling a more comprehensive and accurate analysis.

2.1. Parameters for Geospatial Analysis

The proposed geospatial analysis at the grid level incorporates the following parameters: demand coverage factors, geographic restriction factors, and the relative influence of neighboring areas with and without electrical load. These parameters provide a comprehensive framework for analyzing spatial interactions and constraints within the grid, as outlined in [27].

2.1.1. Coverage Factor (C)

Electrical grids consist of areas designated for consumption, such as residential, commercial, and industrial zones, as well as areas where no consumption is expected, including archaeological sites, parks, and other protected or non-inhabitable regions. Figure 2a illustrates various scenarios: grids with a coverage factor of zero, corresponding to uninhabitable terrains such as hills where no consumption is anticipated; grids with a factor of one, representing fully occupied areas dedicated entirely to consumption; and mixed-use grids with coverage factors less than one, indicating partial occupation or a combination of consumptive and non-consumptive areas.

The coverage factor was determined using the GIS database provided by the distribution company through the following steps. First, the GIS database was analyzed to extract cadastral shapes representing the entire area under the distributor's coverage.

Subsequently, shapes corresponding to the grids of segments S1, S2, and S3 were generated. An overlay operation was then performed between the cadastral shapes and the specified grids to identify polygons within each grid and calculate their respective areas. Finally, the coverage factor for each grid was determined by dividing the total area of the polygons by the area of the corresponding grid, as illustrated in Figure 2b for four cases of segment S1 (100 m side grids).

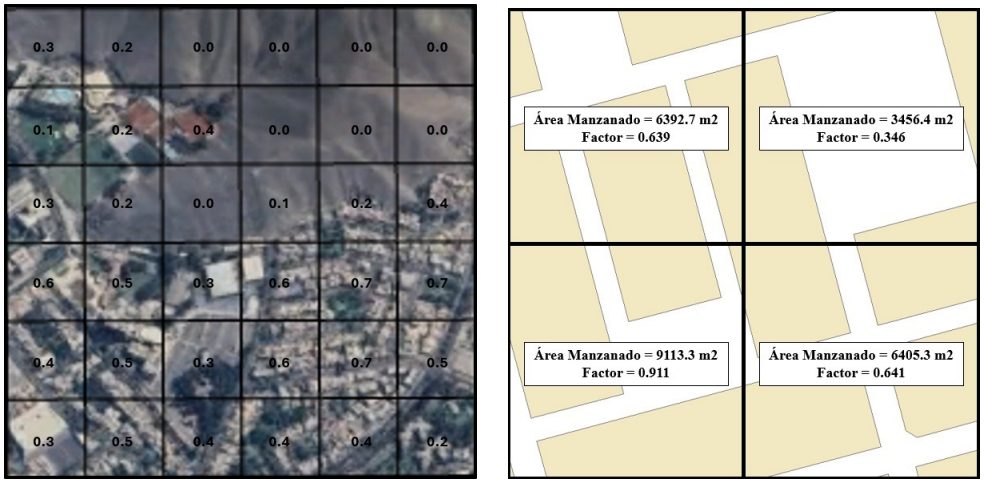

(**a**) (**b**)

Figure 2. Coverage factor. (**a**): Coverage factor in grids; (**b**): coverage factor calculation S3: 100 m.

2.1.2. Constraints (R)

Grids encompassing areas where energy consumption is not anticipated—such as archaeological sites, water bodies (e.g., lakes and rivers), parks, hills, and other similar regions—are assigned a factor of 0. In contrast, grids representing areas with expected energy consumption are assigned a factor of 1. This classification can be specified manually by the user or automatically extracted from a Geographic Information System (GIS), as illustrated in Figure 3.

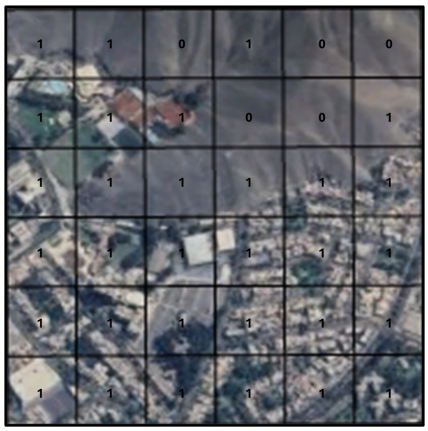

Figure 3. Constraints factor.

2.1.3. Attraction Poles (E.L)

Developed regions exert a significant underlying force that drives growth in surrounding areas. Populations tend to settle as close as possible to zones offering enhanced economic opportunities, access to services, quality of life, education, modernization, and technological advancements. This phenomenon, observable at various scales, is frequently modeled using gravity-center frameworks, also referred to as growth pole models. These

models typically assume that a pole's influence diminishes inversely with distance, with the strongest impact occurring in adjacent areas.

Attraction poles, such as city centers, airports, industrial parks, and similar entities, represent focal points of growth. In large metropolitan areas, multiple attraction poles often coexist and can be modeled at varying scales. In the proposal, the influence of the poles of attraction is represented mathematically through the relative growth (E.L) of the grids in segments S1, S2, and S3, as illustrated in Figure 4 for segment S1.

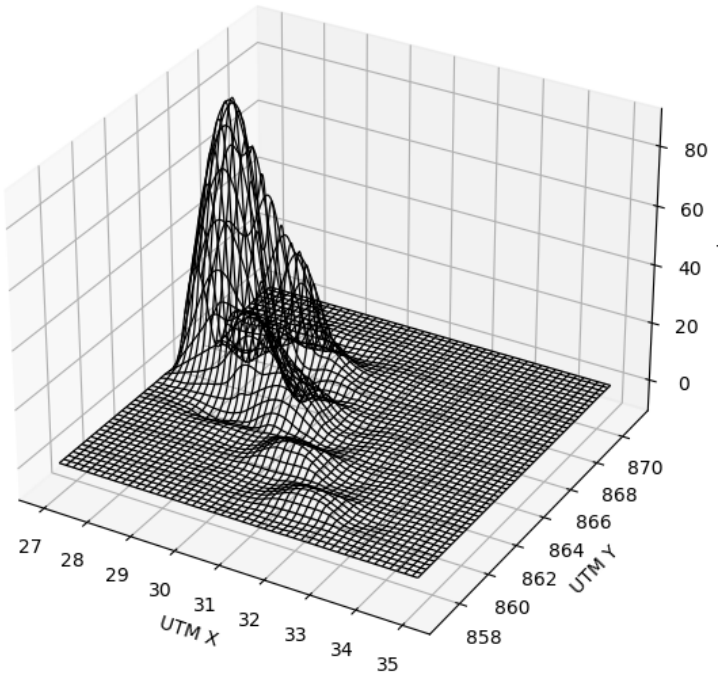

Figure 4. Attraction poles.

2.1.4. Convolution Kernel (M)

The convolution kernel is represented mathematically by a matrix of order $[2N-1]$. The matrix illustrates the influence of the neighboring grids on the growth in the center, including its own.

$$M = \begin{bmatrix} 1 & 1 & 1 \\ 1 & 1 & 1 \\ 1 & 1 & 1 \end{bmatrix} = \begin{bmatrix} 1 & 1 & 1 & 1 & 1 \\ 1 & 1 & 1 & 1 & 1 \\ 1 & 1 & 1 & 1 & 1 \\ 1 & 1 & 1 & 1 & 1 \\ 1 & 1 & 1 & 1 & 1 \end{bmatrix} = \begin{bmatrix} 1 & 1 & 1 & 1 & 1 & 1 & 1 \\ 1 & 1 & 1 & 1 & 1 & 1 & 1 \\ 1 & 1 & 1 & 1 & 1 & 1 & 1 \\ 1 & 1 & 1 & 1 & 1 & 1 & 1 \\ 1 & 1 & 1 & 1 & 1 & 1 & 1 \\ 1 & 1 & 1 & 1 & 1 & 1 & 1 \\ 1 & 1 & 1 & 1 & 1 & 1 & 1 \end{bmatrix} \ldots$$

For the spatial analysis, the kernels with N = 1, 2, 3, and 4 are analyzed and the metrics R2, MAE, RMSE, MAPE, and WAPE are evaluated to assess their efficiency in forecasting.

2.2. Machine Learning Methods

2.2.1. Clustering

Before applying the clustering algorithm, it is imperative to preprocess and normalize the data to ensure meaningful and robust results. Preprocessing and normalization techniques standardize the data, reduce noise and outliers, and eliminate irrelevant or redundant features. In this research, data preprocessing involved cleaning the dataset using an outlier detection and removal method, selecting the most relevant features for

clustering based on the correlation coefficient method, and applying Z-score normalization to transform the features into a consistent scale.

The clustering algorithm used is K-means, recognized for its accuracy and efficiency [28]. The primary mechanism of K-means employs the Euclidean distance as a similarity measure, assigning data points to the nearest centroid by minimizing the distance within clusters. Additionally, the algorithm identifies discrete outliers and groups them into distinct clusters. The objective function for K-means is represented as:

$$\min_{S} E(u_i) = \min_{S} \sum_{i=1}^{k} \sum_{Zc_j \in S_i} \|Zc_j - u_i\|^2$$

Let S denote the dataset, where each element (Zc_j) corresponds to the historical trends of the electrical grids. The dataset is partitioned into k clusters, with each cluster characterized by a centroid (μ_i). To identify the optimal number of clusters, the elbow method and silhouette analysis are applied, ensuring a robust and reliable clustering configuration.

2.2.2. Forecast

The Prophet method is proposed to determine the relative growth of the grids. Prophet is designed to automatically detect seasonality and trends while offering user-friendly parameters without requiring extensive expertise in time series analysis. Prophet implements an additive model with the following components:

$$E(t) = g(t) + s(t) + h(t) + \varepsilon(t)$$

where:

- $E(t)$ represents energy consumption;
- $g(t)$ is the trend function modeling non-periodic changes in the mean value of the time series, describing long-term behavior;
- $s(t)$ is the seasonal component representing periodic changes of known periods (e.g., monthly), modeled using the Fourier series;
- $h(t)$ accounts for the effect of irregular events impacting the series (e.g., COVID-19);
- $\varepsilon(t)$ represents the random component or error term, capturing any changes not accounted for by the other components.

2.3. Convolution

Given a matrix $A \in \mathbb{R}^{n \times m}$ and a matrix $M \in \mathbb{R}^{2n'+1 \times 2m'+1}$, the convolution of matrices A and M is defined as a new matrix $B = A * M$, formulated by the expression:

$$B_{i,j} = \sum_{i'=\underline{i}}^{\bar{i}} \sum_{j'=\underline{j}}^{\bar{j}} A_{i',j'} \, M_{i'-i+n'+1, j'-j+m'+1} \tag{1}$$

where i' and j' are index elements surrounding $A_{i,j}$, bounded by the size of A as follows:

$$\underline{i} = \max\{1, i - n'\}, \quad \bar{i} = \min\{n, i + n'\}$$
$$\underline{j} = \max\{1, j - m'\}, \quad \bar{j} = \min\{m, j + m'\}$$

The matrix M is referred to as the kernel of the convolution. A simple example is illustrated in Figure 5a.

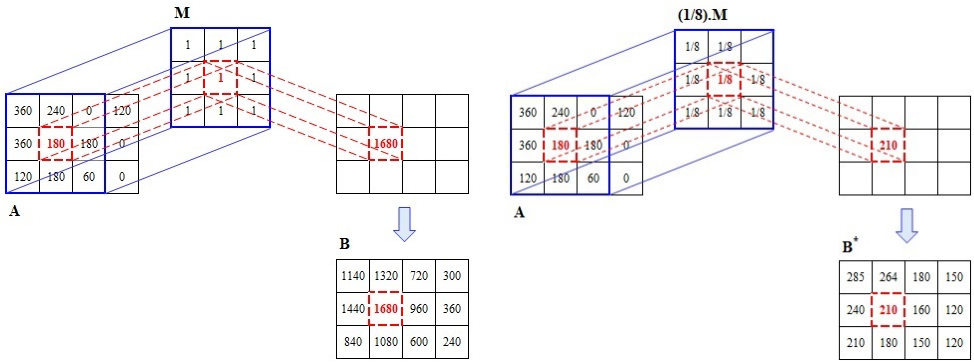

Figure 5. Matrix convolution. (**a**): Standard convolution (unweighted kernel); (**b**): weighted convolution.

Weighted Convolution

To improve the spatial analysis, especially for areas with restrictions equal to 0 and future areas without energy consumption, it is proposed to incorporate a weighting factor, $1/k$, to the above equation. In the example in Figure 5b, the weighting factor is $1/8$.

$$B^{*}_{i,j} = \frac{1}{k} \sum_{i'=\underline{i}}^{\bar{i}} \sum_{j'=\underline{j}}^{\bar{j}} A_{i',j'} M_{(i'-i+n'+1),(j'-j+m'+1)} \tag{2}$$

where:

$$k = \sum k_{i,j} \quad (k_{i,j} = 0 \text{ if } A_{i,j} = 0 \text{ and } k_{i,j} = 1 \text{ if } A_{i,j} > 0)$$

This factor allows for greater emphasis on growth areas and aligns with the actual development patterns of cities.

3. Proposed Method

For the analysis of electricity forecasting in distribution systems, a geospatial demand forecasting method is proposed. This method employs a segmentation process that considers grid maps from the largest to the smallest scale, integrating machine learning and convolution methods. It is designed for application in large-scale systems and accounts for the overall growth of the system across short-, medium-, and long-term horizons. The proposed approach facilitates the processing of large-scale data and their integration with the global forecast, where the cell length at each stage corresponds to the elements of the electrical network. A simplified schematic representation of this method is presented in Figure 6.

1. **Global forecasting:** this refers to estimates made by the distributor at the total system level and serves as a reference for geospatial analysis. Over the years, total system-level forecasting studies have evolved significantly, with abundant literature highlighting diverse approaches. Each author emphasizes the importance of explanatory variables, their selection, and their application through statistical or artificial intelligence methods. This research does not aim to analyze or discuss these methods but focuses on geospatial forecasting.
2. **Supply database:** contains information on the consumption of all clients and their geographical location. This database will be used to determine consumption within the defined grids.
3. **Geographic Information System (GIS):** includes the development of the distribution network and the territorial cadastre within the area served by the distributor. This will form the basis for determining coverage factors and consumption constraints within the grids.

4. **Global forecast estimate:** using the data from point 2, the global forecast can be obtained using the `Prophet` method. For spatial analysis, a choice must be made between this result and the data from point 1. In this study, it will serve as an input variable. In the proposed geospatial analysis, the results of segment S_1 must be adjusted using the global forecast ($N = 1$). Similarly, the results of segments S_2 and S_3 must be adjusted using the outcomes of segments S_1 and S_2, respectively (see Figure 7).
5. **Definition of number of segments (NS) and scales:** the analysis considers different geospatial scales. Smaller grid sizes (e.g., 100 m, 50 m) often result in historical energy consumption data with low correlations, limiting the applicability of existing methods in the literature.
6. **Segmentation process:** this step involves determining the historical consumption of grids at various scales and preparing the database for clustering and relative growth estimation. Additionally, it includes the necessary matrix arrangements for geospatial analysis. This article proposes a three-stage segmentation approach: segment **S1** with a scale of 1:10,000, segment **S2** with a scale of 1:1000, and segment **S3** with a scale of 1:100. To achieve this, the locations of energy supplies are mapped to the corresponding grids for each segment, using their geographic coordinates: **S1** with a resolution of 10^4 m (**C10,000**: UTM/10,000), **S2** with a resolution of 10^3 m (**C1000**: UTM/1000), and **S3** with a resolution of 10^2 m (**C100**: UTM/100). The historical energy consumption within each grid ($\mathbf{Z_c}$) is calculated by summing the consumption of all supplies located within it, providing the foundation for clustering and forecasting processes.
7. **Clustering process:** conducted for each segment using the `K-means` algorithm to determine the optimal number of clusters.
   Before applying the algorithm, detecting and removing outliers is crucial, evaluating features through the correlation coefficient, and performing normalization. The elbow and silhouette methods were utilized for optimal clustering of areas with complete historical data due to their simplicity, computational efficiency, and ease of interpretation. For regions with incomplete historical data, a specific group previously identified was assigned through a training process and confidence intervals. Compared with other evaluated methods, DBSCAN was not practical due to its computational inefficiency and the lack of consistent clustering. Additionally, the processing time for Gaussian Mixture Models was significantly longer, making their use less efficient. On the other hand, employing more complex algorithms such as Random Forest or neural networks did not offer significant benefits at this stage due to the increased computational load.
8. **Relative growth estimation:** for each cluster of grids resulting from the previous process, relative growth is estimated using the `Prophet` method.
   Prophet was selected due to its outstanding balance between accuracy and simplicity in time series analysis, particularly in contexts similar to electrical demand forecasting. It is intuitive and robust against missing data, easily adjustable, and effective when data exhibit clear trends and seasonal effects. Prophet replaces more sophisticated models such as LSTM, which requires a larger data set, more tuning time, and careful hyperparameter configuration, or ARIMA and SARIMA models, which face limitations in handling series with multiple seasonalities or dynamic trends. In this study, the comparison of reported errors confirms that Prophet achieves competitive performance, and its selection is justified by the problem's characteristics and the available resources.
9. **Geospatial analysis:** geospatial analysis involves the application of the convolution algorithm and its subsequent normalization or adjustment based on the results of

the global forecast (EG). The fundamental concept behind the convolution of relative growth ($T.E$) with attraction poles (M) is to determine a reference growth (G) for geospatial forecasting, prior to normalization. Since the convolution process includes grids with restricted areas (R) and areas that are partially or fully covered (C), these parameters must be incorporated into the determination of G. The proposed formulation is expressed in the following equation:

$$G = C \cdot R \cdot [(T.E) * M]$$

Subsequently, this reference growth is normalized to ensure that the globally forecasted growth (ΔEG) matches the total growth of the grids within each segment. The mathematical formulation used for normalization is expressed as follows:

$$E' = E + \frac{\Delta EG}{\sum_i \sum_j G_{i,j}} \cdot G$$

where ΔE represents the growth matrix for the grids in segments $S1$, $S2$, and $S3$. Specifically:

$$\Delta E = E - E' = \sum_{i \in S} \sum_{j \in S} \left(E'_{i,j} - E_{i,j} \right)$$

New consumption grids are identified when the forecast exceeds the historical average obtained based on the statistics of the distribution company.

10. **Final outputs:** the results of geospatial forecasting at the grid level and for each segment.

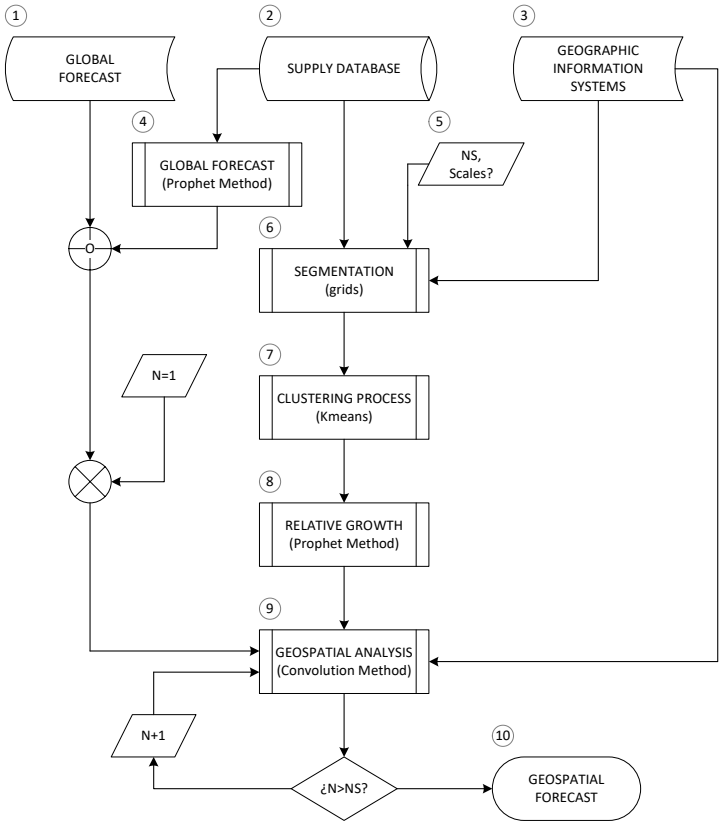

Figure 6. Flowchart of the proposed method.

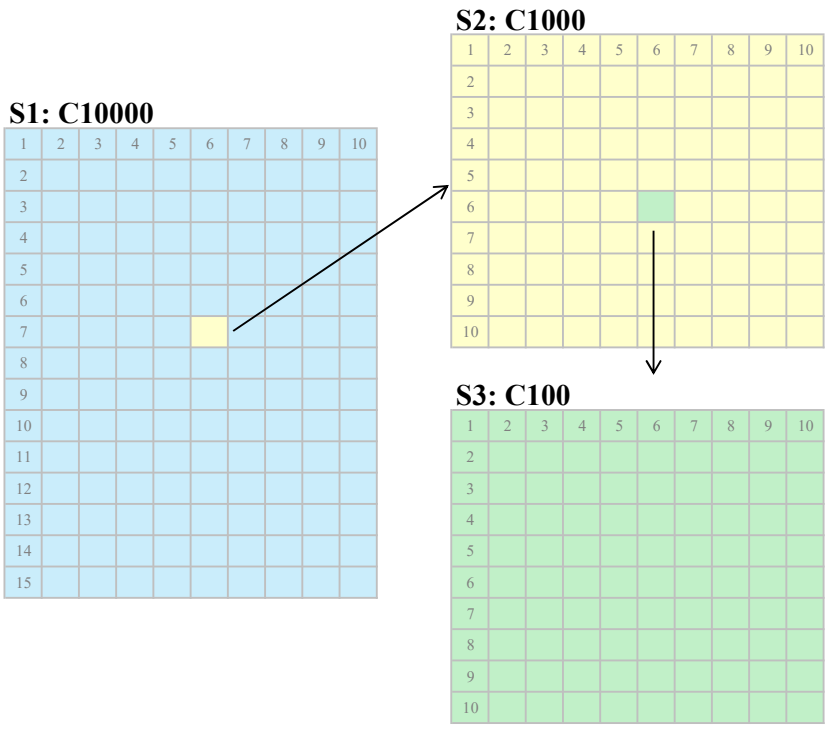

Figure 7. Grid C10,000, C1000, and C100 in segments S1, S2, and S3.

3.1. Simple Application

The initial consumption of an area composed of 12 grids, represented by the matrix $E_{3\times4}$, is 3000 MWh, and the details are as follows:

$$E = \begin{bmatrix} 450 & 300 & 0 & 150 \\ 600 & 300 & 300 & 0 \\ 300 & 450 & 150 & 0 \end{bmatrix} \text{MWh}$$

A global growth of 50% is anticipated over a time horizon.

3.1.1. Spatial Forecasting with Global Growth Rate (EG)

Considering this growth, the projected global consumption would be 4500 MWh ($\Delta E' = 1500$ MWh). In the scenario of scarce historical information at grid level, the resulting growth would be homogeneous, as shown below:

$$E = \begin{bmatrix} 675 & 450 & 0 & 225 \\ 900 & 450 & 450 & 0 \\ 450 & 675 & 2250 & 0 \end{bmatrix} \text{MWh}$$

3.1.2. Spatial Forecasting with Relative Growth Rate (T)

In a real scenario, the growth in the grids is heterogeneous. In this context, for a scenario of relative growth T:

$$T = \begin{bmatrix} 80\% & 80\% & 0\% & 80\% \\ 60\% & 60\% & 60\% & 0\% \\ 40\% & 40\% & 40\% & 0\% \end{bmatrix}$$

The total projected consumption would be 4800 MWh. This result is 10% more than that obtained considering global growth ($\Delta E_r = 1800$ MWh).

$$T \cdot E = \begin{bmatrix} 360 & 240 & 0 & 120 \\ 360 & 180 & 180 & 0 \\ 120 & 180 & 60 & 0 \end{bmatrix} \text{ MWh}$$

Therefore, it is necessary to make the necessary adjustments to normalize it with the global forecast:

$$E' = E + \frac{\Delta E}{\Delta E_r}(T \cdot E) = \begin{bmatrix} 750 & 500 & 0 & 250 \\ 900 & 450 & 450 & 0 \\ 400 & 600 & 200 & 0 \end{bmatrix} \text{ MWh}$$

3.1.3. Geospatial Forecasting Using Convolution

Additionally, in a real scenario, new areas are served due to horizontal growth. In the example, these areas include the grids $E(1,3)$, $E(2,4)$, and $E(3,4)$. To solve this problem, the following parameters are considered in the example: M, C, and R.

$$M = \begin{bmatrix} 1 & 1 & 1 \\ 1 & 1 & 1 \\ 1 & 1 & 1 \end{bmatrix}$$

$$C = \begin{bmatrix} 100\% & 100\% & 80\% & 80\% \\ 100\% & 80\% & 90\% & 90\% \\ 80\% & 80\% & 90\% & 0\% \end{bmatrix}$$

$$R = \begin{bmatrix} 1 & 1 & 1 & 1 \\ 0 & 1 & 1 & 1 \\ 1 & 1 & 1 & 0 \end{bmatrix}$$

where $R(0,1)$ represents an area that is saturated and not growing, and $R(3,4)$ corresponds to an area occupied by a river.

Convolution

$$(T \cdot E) * M = \begin{bmatrix} 285 & 264 & 180 & 150 \\ 240 & 210 & 160 & 120 \\ 210 & 180 & 150 & 120 \end{bmatrix} \text{ MWh}$$

Reference Growth (W)

$$W = C \cdot R \cdot [(T \cdot E) * M] = \begin{bmatrix} 285 & 264 & 144 & 120 \\ 0 & 168 & 144 & 108 \\ 168 & 144 & 135 & 0 \end{bmatrix} \text{ MWh}$$

In total, this amounts to 1680 MWh, which represents a 6% increase over the global forecast.

Final Adjustment

Finally, an adjustment is made to these results to reach the total forecast:

$$E' = E + \frac{\Delta E}{\sum_i \sum_j R_{i,j}} \cdot W = \begin{bmatrix} 704 & 536 & 129 & 257 \\ 600 & 450 & 429 & 96 \\ 450 & 579 & 270 & 0 \end{bmatrix} \text{MWh}$$

3.2. Error Measurement

The spatial forecast error is measured using the following metrics: Coefficient of determination (R2), Mean Absolute Error (MAE), Mean Squared Error (MSE), Root Mean Squared Error (RMSE), Mean Absolute Percentage Error (MAPE), and Weighted Absolute Percentage Error (WAPE). These metrics are defined as follows:

$$\hat{\varepsilon}_{\text{R2}} = 1 - \frac{\sum_{i=1}^{n} \sum_{j=1}^{m} (e_{ij})^2}{\sum_{i=1}^{n} \sum_{j=1}^{m} (E_{ij} - \hat{E})^2}$$

$$\hat{\varepsilon}_{\text{MAE}} = \frac{1}{mn} \sum_{i=1}^{n} \sum_{j=1}^{m} |e_{ij}|$$

$$\hat{\varepsilon}_{\text{MSE}} = \frac{1}{mn} \sum_{i=1}^{n} \sum_{j=1}^{m} (e_{ij})^2$$

$$\hat{\varepsilon}_{\text{RMSE}} = \sqrt{\frac{1}{mn} \sum_{i=1}^{n} \sum_{j=1}^{m} (e_{ij})^2}$$

$$\hat{\varepsilon}_{\text{MAPE}} = \frac{1}{mn} \sum_{i=1}^{n} \sum_{j=1}^{m} |\%e_{ij}|$$

$$\hat{\varepsilon}_{\text{WAPE}} = \frac{\sum_{i=1}^{n} \sum_{j=1}^{m} |\%e_{ij}|}{\sum_{i=1}^{n} \sum_{j=1}^{m} E_{ij}}$$

where:

- e_{ij} denotes the error value at grid cell (i, j);
- E_{ij} denotes the actual value at grid cell (i, j);
- $\hat{E}$ represents the average value of the grid cells;
- n and m are the dimensions of the spatial grid.

These metrics provide valuable insights into the accuracy and reliability of the spatial forecasting model, helping to assess its performance effectively.

4. Validation

In this section, the proposed method is validated in a Peruvian electrical distribution system, whose served area is illustrated in Figure 8. For validation, historical data from the period 2007–2017 are considered for training the models and the period 2018–2023 is projected, comparing the results obtained with the actual values recorded in the same period.

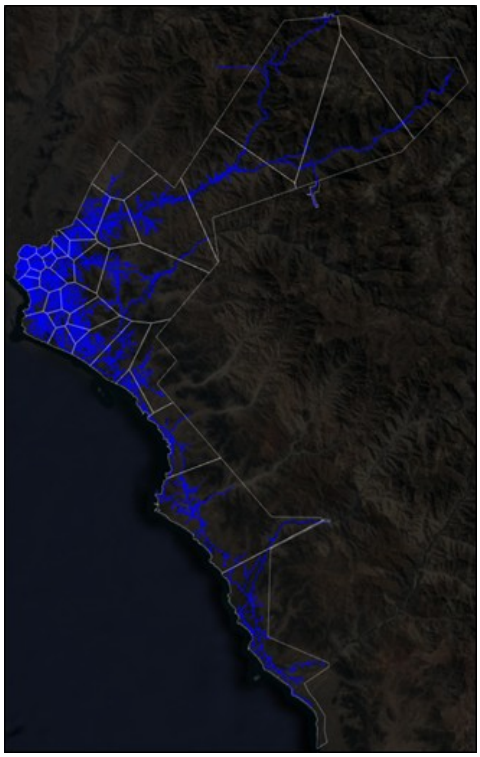

Figure 8. Area served by the "*Lima Sur*" electrical distribution system.

The number of users and historical consumption considered in the analysis is shown in Table 1.

Table 1. Global energy consumption and number of supplies during the period 2007–2023.

Year	Energy Consumption (GWh)	Number of Supplies
2007	4573	739,832
2008	4942	767,013
2009	5774	795,316
2010	6285	824,621
2011	6721	859,094
2012	7162	890,984
2013	7547	924,800
2014	8120	957,574
2015	8239	984,299
2016	8653	1,012,234
2017	8633	1,041,790
2018	8910	1,074,496
2019	9233	1,109,807
2020	8930	1,130,554
2021	8586	1,176,210
2022	9095	1,215,024
2023	9394	1,255,141

The data in Table 1 show the impact on energy consumption in 2020 and 2021 due to the pandemic caused by COVID-19 and its recovery in 2022 and 2023. For validation, the real global growth recorded year-on-year in the period 2018–2023 is considered.

4.1. Segmentation and Clustering

Table 2 highlights two groups within segments S1, S2, and S3: grids with energy consumption records for the entire period from 2007 to 2023 (complete data) and grids that began recording consumption after 2007 (incomplete data).

Table 2. Number of grids in segments S1, S2, and S3.

Year	Grids with Consumption			New Grids		
	S1: C10,000	**S2: C1000**	**S3: C100**	**S1: C10,000**	**S2: C1000**	**S3: C100**
2007	41	888	32,038			
2008	41	895	32,471	0	7	433
2009	41	906	33,040	0	11	569
2010	41	920	33,578	0	14	538
2011	41	930	34,180	0	10	602
2012	41	938	34,623	0	8	443
2013	41	942	35,158	0	4	535
2014	41	948	35,596	0	6	438
2015	41	955	35,859	0	7	263
2016	41	966	36,197	0	11	338
2017	41	980	36,667	0	14	470
2018	41	986	37,089	0	6	422
2019	42	1006	37,630	1	20	541
2020	42	1016	37,950	0	10	320
2021	42	1027	38,919	0	11	969
2022	42	1040	39,577	0	13	658
2023	42	1061	40,357	0	21	780

The data in Table 2 reveal that, within segment S1, consumption was recorded in a new grid starting in 2009. In contrast, segments S2 and S3 incorporated 173 and 8319 new grids, respectively, during the period 2008–2023. Figure 9 highlights the new areas in segments S1, S2, and S3 in blue. In these grids, the initial consumption recorded represents on average 1% of the consumption in the surrounding areas.

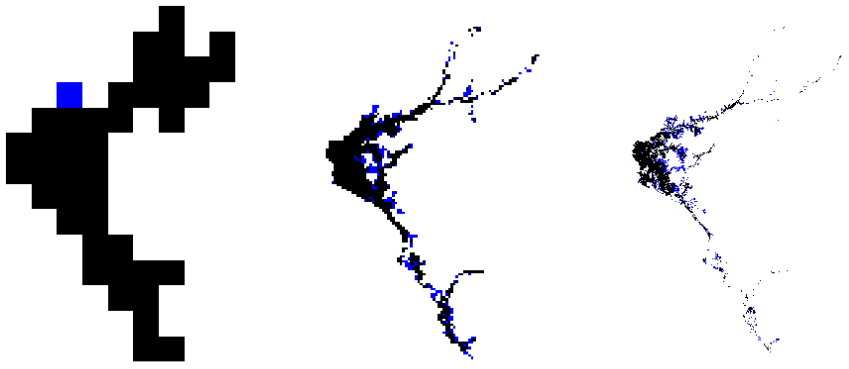

(**a**) (**b**) (**c**)

Figure 9. Consumption grids. (**a**): Segment S1; (**b**): segment S2; (**c**): segment S3.

The analysis results of the historical consumption behavior across the grids for the period 2007–2017 are presented in Table 3. This table categorizes the grids by segment, identifying those with complete and incomplete data. Additionally, it lists the number of outliers and specifies the sample size to be considered for clustering purposes.

Table 3. Analysis of historical consumption in grids.

Grids	Complete Data			Incomplete Data		
	S1: C10,000	S2: C1000	S3: C100	S1: C10,000	S2: C1000	S3: C100
Total	41	885	31,943	0	95	4773
Outliers	8	76	1578	0	24	637
Clusters	33	809	30,365	0	71	4136

The results of the clustering of grids in segments S1, S2, and S3 are shown in Table 4.

Table 4. Clustering results.

Groups	S1: C10,000	S2: C1000	S3: C100
Optimal	6	7	14
Outliers	1	1	1
Total	7	8	15

4.2. Parameters for Geospatial Analysis in Segment S1

The following tables present the base spatial energy (E), consumption groups, annual relative growth rate (T), coverage factors (C) and restrictions (R) for segment S1. A similar procedure is applied for segments S2 and S3.

The spatial analysis to forecast consumption in 2018–2023 is carried out sequentially each year. Table 5 contains the energy for the base year recorded in 2017 and the consumption groups obtained for segment S1. In this context, *X* and *Y* represent the UTM Easting and Northing coordinates, respectively, scaled to 1:10,000.

Regarding the last column labeled "36", it is suggested to remove or eliminate it across all tables, specifically Tables 5, 7, 9 and 10.

Table 5. Base energy (E) and consumption groups.

Baseline Energy: 2017											Consumption Groups									
Y↓/X→	**27**	**28**	**29**	**30**	**31**	**32**	**33**	**34**	**35**	**36**	**Y↓/X→**	**27**	**28**	**29**	**30**	**31**	**32**	**33**	**34**	**35**	**36**
871							0.5				871							1			
870						0.2	0.0		5.2		870						1	5		7	
869						0.7	0.0	1.3	1.1		869						5	5	5	7	
868					40.4	3.3	1.6	5.2			868			1		5	2	2	5		
867		62.8	585.1	162.5	25.9		0.2				867		1	6	2	2		2			
866	963.5	2891.6	204.9	22.4							866	2	2	2	1						
865	351.9	1560.1	370.5	6.3							865	2	2	7	6						
864		201.6	498.8	226.2							864		1	6	4						
863			9.3	133.6							863			7	7						
862				12.1	9.7						862				1	1					
861				5.7	84.6	0.3	0.6				861				1	7	3	3			
860					5.0	16.4					860					6	2				
859						135.3					859						7				
858						19.8	6.9				858						2	7			
857											857										

Table 6 shows the relative growth rates of the consumption groups of segment S1 obtained for the period 2018–2023.

Table 6. Relative growth rate in consumption groups of segment S1 (T).

Group	2018	2019	2020	2021	2022	2023
1	6.4%	6.0%	5.7%	5.4%	5.1%	4.8%
2	2.0%	1.9%	1.8%	1.9%	1.8%	1.8%
3	9.0%	8.3%	7.6%	7.1%	6.6%	6.2%
4	8.5%	7.7%	7.0%	6.9%	6.3%	5.9%
5	−0.1%	−0.2%	−0.6%	0.2%	−0.2%	−0.2%
6	1.1%	1.0%	1.0%	1.0%	1.0%	1.0%
7	4.9%	4.0%	3.3%	4.4%	3.6%	3.5%

Table 7 presents the coverage and restriction factors obtained for the grids in segment S1. The tables emphasize the factors related to new areas that should be considered for horizontal growth. The areas highlighted in blue indicate regions where future energy consumption is anticipated. Conversely, in the remaining areas, future energy consumption would not be feasible, resulting in a restriction factor of zero. Regarding the coverage factors, an estimate of 2.0% has been assigned, as the majority of these areas are covered by rocky mountains.

Table 8 shows the energy consumption in the grids for the training and validation period.

Table 7. Coverage factor (C) and constraints (R).

	Coverage Factor										Constraints									
Y↓/X→	27	28	29	30	31	32	33	34	35	36	Y↓/X→	27	28	29	30	31	32	33	34	35	36
871							0.2%				871							1			
870						0.1%	0.0%		0.1%		870						1	1		1	
869				2.0%		0.2%	0.0%	0.2%	0.2%		869				**1**		1	1	1	1	
868			2.4%		3.7%	1.2%	0.3%	0.2%			868			1		1	1	1	1		
867		4.6%	25.2%	12.6%	4.2%		0.1%				867		1	1	1	1		1			
866	11.7%	48.3%	21.6%	5.7%							866	1	1	1	1						
865	3.4%	58.0%	15.7%	2.6%							865	1	1	1	1						
864		14.8%	41.0%	7.6%	2.0%						864		1	1	1	**1**					
863			0.6%	6.8%	2.0%						863			1	1	**1**					
862				3.8%	2.9%	2.0%					862				1	1	**1**				
861				2.1%	8.0%	0.1%	0.2%				861				1	1	1	1			
860					0.5%	2.7%					860					1	1				
859						4.6%					859						1				
858						2.0%	4.2%				858						1	1			
857							2.0%				857							**1**			

Table 8. Energy consumption in S1 grids (GWh).

S1	Model Training Period											Model Validation						
C10,000	2007	2008	2009	2010	2011	2012	2013	2014	2015	2016	2017	2018	2019	2020	2021	2022	2023
27-865	225	243	263	278	289	306	318	328	341	361	352	352	362	319	285	316	345
27-866	638	682	709	763	822	867	876	904	937	986	963	973	999	904	801	872	960
28-864	81	95	99	113	124	135	153	166	173	188	202	213	225	239	233	244	265
28-865	940	1012	1055	1118	1191	1269	1334	1400	1444	1532	1560	1618	1682	1798	1583	1616	1703
28-866	1814	1919	2133	2306	2422	2535	2662	2784	2789	2919	2892	2912	2966	2746	2575	2738	2841
28-867	30	32	32	36	39	43	47	52	56	62	63	69	72	71	82	86	87
29-863	2	2	2	2	2	2	3	3	5	8	9	9	11	17	16	16	15
29-864	203	224	231	266	321	384	422	478	475	488	499	525	545	579	560	572	559
29-865	33	37	347	366	354	344	337	465	417	396	370	402	440	327	456	484	437
29-866	117	129	139	149	160	166	175	183	191	203	205	213	220	252	227	230	242
29-867	194	230	289	353	397	453	508	565	586	616	585	622	656	632	661	710	718

Table 8. *Cont.*

S1	Model Training Period										Model Validation						
C10,000	**2007**	**2008**	**2009**	**2010**	**2011**	**2012**	**2013**	**2014**	**2015**	**2016**	**2017**	**2018**	**2019**	**2020**	**2021**	**2022**	**2023**
29-868													15	16	16	18	18
30-861	2	2	3	3	3	3	3	4	4	6	6	6	7	8	8	12	14
30-862	6	6	7	7	8	9	10	11	11	12	12	13	13	17	16	16	16
30-863	22	22	50	62	77	80	92	125	122	131	134	144	144	135	155	173	159
30-864	42	66	71	86	88	112	156	175	193	212	226	242	238	212	252	281	287
30-865	2	3	3	4	4	5	6	6	6	6	6	7	7	8	8	8	8
30-866	11	12	13	14	15	16	18	19	20	22	22	24	25	29	28	28	29
30-867	103	114	123	130	139	148	154	164	167	167	163	171	179	192	187	195	197
31-860	2	2	2	2	3	3	3	4	4	5	5	5	6	6	6	6	7
31-861	9	10	11	11	13	16	20	27	40	65	85	100	120	112	132	138	144
31-862	2	3	3	3	4	4	4	4	5	6	10	14	17	15	18	21	21
31-867	18	19	20	22	23	23	24	25	26	27	26	27	28	31	28	29	29
31-868	30	32	33	35	36	37	40	41	41	42	40	41	42	47	42	42	41
32-858	10	11	12	12	13	14	15	16	17	18	20	19	19	21	21	20	22
32-859	14	11	97	105	114	119	119	132	127	130	135	140	140	136	135	164	168
32-860	8	9	10	11	12	12	13	15	16	16	16	17	19	22	19	20	21
32-861	0	0	0	0	0	0	0	0	0	0	0	0	0	1	1	1	1
32-868	2	2	2	2	2	3	3	3	3	3	3	4	4	4	4	5	8
32-869	1	1	1	1	1	1	1	1	1	1	1	1	1	1	1	1	1
32-870	0	0	0	0	0	0	0	0	0	0	0	0	0	0	0	0	0
33-858	2	2	2	3	4	5	6	6	6	7	7	8	8	9	9	10	10
33-861	0	0	0	0	0	0	0	1	1	1	1	1	1	1	1	1	1
33-867	0	0	0	0	0	0	0	0	0	0	0	0	0	0	0	0	0
33-868	1	1	1	1	1	1	1	1	2	2	2	2	2	2	2	2	2
33-869	0	0	0	0	0	0	0	0	0	0	0	0	0	0	0	0	0
33-870	0	0	0	0	0	0	0	0	0	0	0	0	0	0	0	0	0
33-871	0	0	0	0	0	0	0	1	1	0	1	1	0	0	1	1	1
34-868	5	5	5	5	5	6	6	6	5	5	5	6	7	7	9	10	9
34-869	1	1	1	1	1	1	1	1	1	1	1	1	1	2	1	1	2
35-869	1	1	1	12	29	32	13	3	1	1	1	3	5	5	4	3	3
35-870	2	2	3	2	2	2	2	4	5	5	5	5	5	3	3	4	4
Total	4573	4942	5774	6285	6721	7162	7547	8120	8239	8653	8633	8910	9233	8930	8586	9095	9394

Finally, for the spatial analysis, the kernels with N = 1, 2, 3, and 4 are analyzed and the metrics R^2, MAE, RMSE, MAPE, and WAPE are evaluated to assess their efficiency in forecasting.

4.3. Geospatial Forecast Results in Segment S1

The analysis was conducted on a year-by-year basis using the proposed formulation through the convolution algorithm, covering the period from 2018 to 2023. Table 9 presents the geospatial forecast for 2018 within segment S1, utilizing the 3×3 core matrix. The table highlights the distribution of energy demand across geospatial coordinates, represented by rows (Y) and columns (X). The results reveal concentrated demand in specific grid cells, particularly along coordinates $Y = 866$ and $Y = 867$, with peaks of 2949.2 GWh and 605.8 GWh, respectively. These high-demand regions correspond to urban or industrial zones, where consumption is typically more intense. In contrast, cells with minimal or zero values indicate sparsely populated or low-consumption areas. The total energy demand for the segment in 2018 amounts to 8910.3 GWh, reflecting the spatial variability inherent in the segment.

The geospatial forecast for 2023, presented in Table 10, provides a detailed distribution of energy demand across a 3×3 core matrix. The forecast highlights significant variability in energy consumption, with notable concentrations in specific geographic zones. The

highest energy demand is observed in cell (866, 28), with a value of 3052.5 GWh, followed by cell (866, 27) at 1014.5 GWh and cell (865, 28) at 1762.4 GWh, indicating densely populated or high-consumption areas. Conversely, the majority of cells show negligible or zero consumption, reflecting sparsely populated or low-demand zones. This spatial distribution underscores the algorithm's ability to identify hotspots of energy usage and allocate resources accordingly. The total projected demand for the region amounts to 9394.2 GWh, providing a comprehensive basis for infrastructure planning and optimization. These results demonstrate the utility of the geospatial forecasting methodology in capturing localized consumption patterns critical for effective energy distribution.

Table 9. Geospatial forecast for 2018: core matrix 3 × 3.

Y↓/X→	27	28	29	30	31	32	33	34	35	36
871	0.0	0.0	0.0	0.0	0.0	0.0	0.5	0.0	0.0	0.0
870	0.0	0.0	0.0	0.0	0.0	0.2	0.0	0.0	5.2	0.0
869	0.0	0.0	0.0	0.0	0.0	0.7	0.0	1.4	1.1	0.0
868	0.0	0.0	0.0	0.0	40.7	3.3	1.6	5.2	0.0	0.0
867	0.0	68.3	605.8	165.0	26.2	0.0	0.2	0.0	0.0	0.0
866	981.4	2949.2	224.5	24.2	0.0	0.0	0.0	0.0	0.0	0.0
865	357.5	1633.0	387.5	7.7	0.0	0.0	0.0	0.0	0.0	0.0
864	0.0	213.5	530.2	230.3	0.0	0.0	0.0	0.0	0.0	0.0
863	0.0	0.0	9.6	136.1	0.0	0.0	0.0	0.0	0.0	0.0
862	0.0	0.0	0.0	12.7	10.1	0.0	0.0	0.0	0.0	0.0
861	0.0	0.0	0.0	5.9	85.0	0.3	0.6	0.0	0.0	0.0
860	0.0	0.0	0.0	0.0	5.1	16.8	0.0	0.0	0.0	0.0
859	0.0	0.0	0.0	0.0	0.0	135.8	0.0	0.0	0.0	0.0
858	0.0	0.0	0.0	0.0	0.0	20.1	7.6	0.0	0.0	0.0
857	0.0	0.0	0.0	0.0	0.0	0.0	0.0	0.0	0.0	0.0
										Total: 8910.3

Table 10. Geospatial forecast for 2023: core matrix 3 × 3 (GWh).

Y↓/X→	27	28	29	30	31	32	33	34	35	36
871	0.0	0.0	0.0	0.0	0.0	0.0	0.5	0.0	0.0	0.0
870	0.0	0.0	0.0	0.0	0.0	0.2	0.0	0.0	5.2	0.0
869	0.0	0.0	0.0	0.0	0.0	0.7	0.0	1.4	1.1	0.0
868	0.0	0.0	1.2	0.0	41.3	3.3	1.6	5.2	0.0	0.0
867	0.0	77.7	642.1	169.4	26.9	0.0	0.2	0.0	0.0	0.0
866	1014.5	3052.5	259.3	27.1	0.0	0.0	0.0	0.0	0.0	0.0
865	367.6	1762.4	416.7	9.8	0.0	0.0	0.0	0.0	0.0	0.0
864	0.0	233.8	581.0	236.5	0.0	0.0	0.0	0.0	0.0	0.0
863	0.0	0.0	10.1	139.9	0.0	0.0	0.0	0.0	0.0	0.0
862	0.0	0.0	0.0	13.5	10.7	0.0	0.0	0.0	0.0	0.0
861	0.0	0.0	0.0	6.2	85.8	0.3	0.6	0.0	0.0	0.0
860	0.0	0.0	0.0	0.0	5.2	17.3	0.0	0.0	0.0	0.0
859	0.0	0.0	0.0	0.0	0.0	136.5	0.0	0.0	0.0	0.0
858	0.0	0.0	0.0	0.0	0.0	20.6	8.6	0.0	0.0	0.0
857	0.0	0.0	0.0	0.0	0.0	0.0	0.0	0.0	0.0	0.0
										Total: 9394.2

Figure 10 highlights, in blue, the new grid areas that recorded electricity consumption during the 2018–2023 period. Specifically, Figure 10a, 10b, and 10c provide details for segments S1, S2, and S3, respectively. In real-world scenarios, such as those illustrated in Figure 10b,c, smaller-scale segments reveal new consumption areas located far from urban zones (isolated regions). These areas are typically associated with industrial loads or regions that previously lacked electrical coverage, particularly in rural distribution systems.

(**a**) (**b**) (**c**)

Figure 10. New grids with real consumption in the period 2018–2023. (**a**): Segment S1; (**b**): segment S2; (**c**): segment S3.

Figure 11 presents the geospatial forecasting results for 2018–2023, depicted in red. Specifically, Figure 11a, 11b, and 11c illustrate the forecasts corresponding to segments S1, S2, and S3, respectively. In Figure 11b,c, it is evident that isolated areas from the real-case scenario were not accurately identified by the convolutional kernels analyzed, which included sizes of 3×3, 5×5, 7×7, and 9×9. For these cases, particularly in smaller-scale segments, it is recommended to explore the use of higher-order kernels to enhance their range and improve forecasting accuracy.

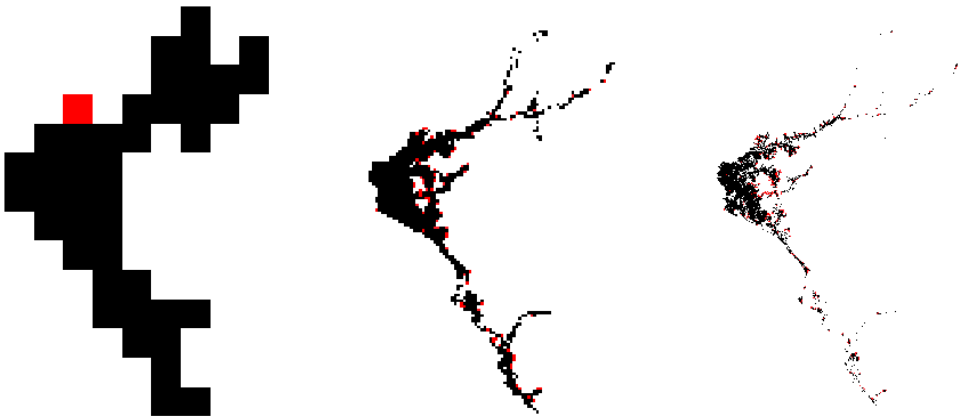

(**a**) (**b**) (**c**)

Figure 11. Forecast of new grids with consumption in the period 2018–2023. (**a**): Segment S1; (**b**): segment S2; (**c**): segment S3.

4.4. Calculation of Metrics

The metrics were determined year-on-year and for the analyzed projection scenarios as follows:

- Spatial forecast considering global growth rates (global).
- Spatial forecast considering growth rates by groups in segments S1, S2, and S3 (zonal).
- Spatial forecasting using standard convolution (spatial [27]).

Additionally, convolution kernels of sizes 3×3, 5×5, 7×7, and 9×9 were incorporated into the proposed methodology. In the measurement tables of the metrics MAE, RMSE, MAPE, and WAPE, the values with the lowest magnitude for each year are highlighted in blue for clarity and emphasis.

The results of the metrics obtained in segment S1 are summarized in Table 11.

Table 11. Calculation of MAE, MSE, RMSE, and MAPE.

Scenario	Grid Size	MAE (GWh)						RMSE (GWh)					
		2018	**2019**	**2020**	**2021**	**2022**	**2023**	**2018**	**2019**	**2020**	**2021**	**2022**	**2023**
Global		5.3	8.8	22.4	25.0	25.5	20.8	13.1	22.7	52.8	58.8	59.3	53.3
Zonal		5.0	9.8	23.1	25.0	23.3	18.1	11.2	20.2	52.4	58.7	55.6	48.0
Spatial [27]		5.3	10.2	21.0	25.6	22.0	19.1	9.2	18.3	47.6	60.4	44.4	33.1
Proposed	3×3	4.3	7.2	19.3	25.3	23.4	18.6	8.4	14.2	45.3	59.2	50.9	40.3
	5×5	3.8	6.5	18.9	25.9	21.2	15.9	7.2	12.8	46.0	60.8	47.8	35.1
	7×7	3.6	6.3	18.8	25.8	21.3	15.5	6.9	11.9	45.7	60.5	47.6	34.6
	9×9	3.5	6.1	18.6	25.7	21.1	15.0	6.6	11.3	45.5	60.3	47.2	33.8
Scenario	**Grid Size**	**MAPE**						**WAPE**					
		2018	**2019**	**2020**	**2021**	**2022**	**2023**	**2018**	**2019**	**2020**	**2021**	**2022**	**2023**
Global		8.0%	13.7%	23.9%	26.2%	25.1%	24.5%	2.4%	4.0%	10.5%	12.2%	11.8%	9.3%
Zonal		7.9%	13.8%	24.0%	26.3%	24.1%	22.9%	2.3%	4.4%	10.9%	12.2%	10.8%	8.1%
Spatial [27]		15.2%	20.8%	20.9%	27.9%	23.9%	24.7%	2.5%	4.6%	9.9%	12.5%	10.2%	8.5%
Proposed	3×3	8.4%	14.6%	23.2%	26.1%	25.3%	25.3%	2.0%	3.3%	9.1%	12.4%	10.8%	8.3%
	5×5	8.7%	14.5%	22.4%	26.7%	24.5%	24.4%	1.8%	2.9%	8.9%	12.6%	9.8%	7.1%
	7×7	8.5%	13.4%	21.1%	27.0%	23.3%	23.1%	1.7%	2.8%	8.8%	12.6%	9.8%	6.9%
	9×9	8.4%	12.3%	18.8%	27.4%	20.8%	19.0%	1.6%	2.8%	8.8%	12.6%	9.8%	6.7%

The data analysis presented in Table 11 highlights the comparative performance of different methodologies and grid sizes regarding the metrics MAE, RMSE, MAPE, and WAPE. The proposed methodology consistently demonstrates superior accuracy compared with the global, zonal, and spatial methods across all metrics and years.

In terms of MAE and RMSE, the proposed 9×9 grid configuration achieves the lowest error values across all years. For instance, in 2018, the 9×9 grid records an MAE of 3.5 GWh and an RMSE of 6.6 GWh, outperforming other grid configurations such as 3×3, 5×5, and 7×7. Similar trends are observed in subsequent years, where the 9×9 grid consistently yields the smallest error margins, demonstrating its effectiveness in capturing demand variations with high precision.

The MAPE values further corroborate the effectiveness of the proposed 9×9 grid. It achieves the lowest percentages in multiple years, particularly in 2019 (12.3%) and 2020 (18.8%). These results highlight the ability of the 9×9 configuration to minimize relative prediction errors, making it a robust choice for accurate energy demand forecasting.

The MAPE is an indicator that is frequently used in demand forecasting because it is easily interpretable. However, in spatial analysis it can be biased when there are divisions by zero, outliers, or due to the scale of the actual values. For example, if a grid with a consumption of 1000 GWh has an error of 1% (10 GWh) and another with a consumption of 10 GWh has an error of 10% (1 GWh), the MAPE of the set would be 5.5%.

The WAPE that weights the errors by the volume of demand is a highly recommended measure since it minimizes the impact of grids with very variable demands. In the example above, the WAPE of the set would be 1.09% = [(10 + 1)/(1000 + 10)], which is more reasonable on a global scale.

The WAPE metric also underlines the advantages of the 9 × 9 grid. It achieves the smallest WAPE percentages, notably 1.6% in 2018 and 6.7% in 2023, indicating its reliability in maintaining low-weighted aggregate prediction errors. Overall, the 9 × 9 grid consistently outperforms other configurations, making it the most effective choice within the proposed methodology.

Finally, Table 12 presents the average values of the MAPE and WAPE metrics obtained for segments S1, S2, and S3 during the periods 2018–2019 and 2018–2023, which include the years affected by the COVID-19 pandemic. The scenario with the lowest metrics is highlighted in blue. The table compares results obtained using standard convolution with a 3 × 3 kernel [27] and weighted convolution for kernels of sizes 3 × 3, 5 × 5, 7 × 7, and 9 × 9. The Global and Zonal scenarios are not included, as these do not forecast new consumption areas, such as those shown in Figure 11 (marked in red).

Table 12. MAPE and WAPE metrics in segments S1, S2, and S3: average for periods 2018–2019 and 2018–2023.

Scenario	Grid Size	MAPE						WAPE					
		Segment S1		Segment S2		Segment S3		Segment S1		Segment S2		Segment S3	
		18–19	18–23	18–19	18–23	18–19	18–23	18–19	18–23	18–19	18–23	18–19	18–23
Spatial [27]		18.0%	22.2%	16.7%	31.4%	16.6%	25.8%	3.5%	8.0%	6.3%	12.8%	12.9%	23.3%
Proposed	3 × 3	11.5%	20.5%	13.9%	26.2%	15.9%	26.9%	2.6%	7.6%	6.1%	12.7%	12.6%	23.2%
	5 × 5	11.6%	20.2%	14.1%	27.4%	16.4%	27.1%	2.4%	7.2%	6.0%	12.5%	12.8%	23.3%
	7 × 7	11.0%	19.4%	14.3%	27.7%	16.7%	26.8%	2.3%	7.1%	5.8%	12.3%	12.8%	23.2%
	9 × 9	10.3%	17.8%	14.6%	27.6%	17.0%	27.3%	2.2%	7.0%	5.8%	12.3%	12.8%	23.2%

The metrics MAPE and WAPE obtained through weighted convolution outperform those obtained through standard convolution, except for the estimate for the period 2018–2023 in segment S3. In segment S1, the proposed method reduces the MAPE by up to 7.7% and the WAPE by up to 1.3% during the period 2018–2019. For the period 2018–2023, the MAPE is reduced by up to 5.6% and the WAPE by up to 1.0%.

Similarly, the MAPE and WAPE metrics for segment S2 increased by over 3% during the period 2018–2019 and by over 5% during 2018–2023. In segment S3, these metrics increased by more than 5% during 2018–2019 and by over 10% during 2018–2023.

5. Long-Term Forecast

This section presents a proposal for spatial energy forecasting over a 20-year horizon, extending to 2043. The results of the global forecast, generated using the Prophet method, are summarized in Table 13. The forecast indicates a steady annual increase in energy consumption, starting at 9659 GWh in 2024 and reaching 14,750 GWh by 2043. The annual growth rates (T.C.) exhibit a gradual decline over the forecast period, decreasing from 2.9% in 2024 to 1.9% in 2043. As previously indicated, this article aims to explore geospatial forecasting in alignment with the global growth of the system. In this context, the results produced by the Prophet model are analyzed; however, in practical applications, the input data would likely be derived from more advanced and efficient methods or techniques. Additionally, alternative scenarios, both pessimistic and optimistic, may also be considered for a more comprehensive analysis.

The relative growth of consumption groups within segment S1 is presented in Table 14. This table provides a detailed overview of the annual growth rates for seven consumption groups from 2024 to 2043. The analysis reveals distinct trends, with Group 1 consistently exhibiting positive growth, albeit at a declining rate, starting from 4.9% in 2024 and tapering to 2.2% in 2043. In contrast, Group 2 shows minimal or negative growth throughout the period, with rates fluctuating between 0.1% and −1.0%, highlighting challenges in this segment. Groups 3, 4, and 5 maintain moderate but steady growth rates, with notable peaks

in the earlier years, such as 4.8%, 7.5%, and 6.8%, respectively, in 2024, before gradually decreasing over time. Groups 6 and 7 demonstrate lower growth rates overall, with values generally remaining below 3.6% and 5.8% in the initial years and tapering to less than 2.0% by 2043. These trends suggest a general deceleration in growth across most groups, emphasizing the need for targeted strategies to address consumption dynamics, particularly for underperforming groups such as Group 2.

Table 13. Global forecast, period 2024–2043.

Año	Energy Consumption (GWh)	T.C.	Año	Energy Consumption (GWh)	T.C.
2024	9659	2.9%	2034	12,339	2.2%
2025	9927	2.8%	2035	12,607	2.2%
2026	10,195	2.7%	2036	12,874	2.1%
2027	10,463	2.6%	2037	13,142	2.1%
2028	10,731	2.6%	2038	13,410	2.0%
2029	10,999	2.5%	2039	13,678	2.0%
2030	11,267	2.4%	2040	13,946	2.0%
2031	11,535	2.4%	2041	14,214	1.9%
2032	11,803	2.3%	2042	14,482	1.9%
2033	12,071	2.3%	2043	14,750	1.9%

Table 14. Reference growth rate for segment S1 consumption groups.

Año	S1 Consumer Groups						
	1	2	3	4	5	6	7
2024	4.9%	0.0%	4.8%	7.5%	6.8%	3.6%	5.8%
2025	4.2%	0.1%	4.0%	6.8%	6.4%	2.8%	4.2%
2026	3.6%	−0.5%	3.3%	6.1%	5.9%	2.1%	3.1%
2027	3.5%	−0.5%	3.2%	5.7%	5.6%	2.1%	3.0%
2028	3.0%	−0.9%	2.7%	5.2%	5.3%	1.6%	2.1%
2029	3.7%	0.1%	3.5%	5.4%	5.1%	2.5%	3.7%
2030	3.2%	−0.5%	2.9%	4.9%	4.8%	2.0%	2.7%
2031	3.1%	−0.5%	2.8%	4.7%	4.6%	1.9%	2.6%
2032	2.7%	−0.9%	2.4%	4.3%	4.3%	1.4%	1.8%
2033	3.2%	0.1%	3.1%	4.4%	4.2%	2.3%	3.3%
2034	2.8%	−0.5%	2.6%	4.1%	4.0%	1.8%	2.5%
2035	2.7%	−0.5%	2.6%	3.9%	3.8%	1.8%	2.4%
2036	2.4%	−0.9%	2.1%	3.6%	3.7%	1.3%	1.7%
2037	2.9%	0.1%	2.8%	3.8%	3.6%	2.2%	3.0%
2038	2.5%	−0.5%	2.4%	3.5%	3.4%	1.7%	2.2%
2039	2.5%	−0.5%	2.3%	3.4%	3.3%	1.7%	2.2%
2040	2.2%	−1.0%	1.9%	3.2%	3.2%	1.3%	1.5%
2041	2.6%	0.1%	2.6%	3.3%	3.2%	2.0%	2.8%
2042	2.3%	−0.5%	2.2%	3.1%	3.0%	1.6%	2.0%
2043	2.2%	−0.5%	2.1%	3.0%	2.9%	1.6%	2.0%

The remaining parameters are held constant for the geospatial analysis.

The spatial forecast presented in Table 15 illustrates the projected energy demand within segment S1 using a 3×3 convolution matrix for a 20-year horizon. The data reveal significant variations in energy consumption across different spatial coordinates, with high-demand zones concentrated in specific areas while others exhibit negligible or no demand. This variation emphasizes the importance of geospatial forecasting in identifying critical zones for targeted infrastructure development and efficient resource allocation.

A detailed examination of Table 15 highlights that rows 866 and 865, particularly in columns 28 and 29, represent areas of peak energy demand, with values reaching 3416.7 GWh and 3772.2 GWh, respectively. These zones are likely indicative of urban or industrial hubs that will continue to drive energy consumption growth in the future. Additionally, localized demand spikes, such as the 745.2 GWh forecast in row 867, column 29, suggest emerging consumption centers that may require strategic interventions to ensure adequate energy supply. Conversely, many regions in the forecast exhibit minimal or zero demand, reflecting underdeveloped or sparsely populated areas where significant growth is not expected within the projection horizon. However, incremental increases in previously low-demand regions, such as the 46.9 GWh forecast in row 868, column 29, indicate the gradual expansion of electrical coverage and development in these zones.

The forecast projects the addition of five new service areas within segment S1 over the 20-year horizon, a marked acceleration compared with the historical trend. Between 2007 and 2023, the distribution company expanded its serviced area by only one grid, achieved in 2019. This forecasted growth highlights the increasing electricity demand and underscores the need for proactive infrastructure planning to meet future consumption requirements.

Table 15. Spatial forecast for the year 2043 in S1—3 × 3 matrix (GWh).

Y↓/X→	27	28	29	30	31	32	33	34	35	36
871							0.6			
870						0.5	0.3		4.6	
869				**4.9**		3.4	0.6	2.3	3.7	
868			46.9		45.7	11.2	3.0	10.2		
867		93.4	745.2	352.6	52.6		2.5			
866	959.6	3416.7	290.9	145.2						
865	347.8	3772.2	722.7	68.9						
864		689.0	1602.0	430.5	**21.7**					
863			61.2	255.6	**17.8**					
862				33.6	33.0	**2.0**				
861				21.2	164.2	5.6	1.1			
860					16.2	33.3				
859						189.0				
858						33.6	34.6			
857							**0.9**			
					14,754.2					

Five (5) new areas, highlighted in blue, were identified due to the spatial analysis. This outcome is optimistic, considering the current level of electrical coverage provided by the distribution company and the historical precedent recorded during the 2007–2023 period, where only one new area was served for 17 years.

However, with the 9 × 9 core matrix, the projection for a 20-year horizon anticipates the inclusion of two (2) new areas in segment S1, with estimated consumption values highlighted in blue, as shown in Table 16. This result aligns more closely with the historical horizontal growth of the distribution company, which expanded its coverage by only one (1) grid square in 2019 during the 2007–2023 period.

The spatial forecast for 2043, presented in Table 16, highlights the predicted energy consumption across various grid segments using the 9 × 9 matrix. The results indicate significant variability in predicted consumption, with certain grid cells exhibiting high demand, while others remain at minimal or zero levels. This variability underscores the importance of spatial granularity in energy demand forecasting, as it enables the identification of critical consumption areas and potential zones for infrastructure development.

Key findings from the forecast include notable energy concentrations in specific segments, such as cells (866, 28), (866, 29), and (865, 28), which show the highest consumption levels of 3607.7 GWh, 1158.2 GWh, and 2582.2 GWh, respectively. These high-demand zones are predominantly situated in areas characterized by urban or industrial growth. In contrast, several cells display zero or negligible demand, indicating either uninhabited regions or areas with limited infrastructure and minimal consumption activity. Highlighted values in blue, such as 16.1 GWh in cell (864, 31) and 17.3 GWh in cell (857, 34), represent smaller yet strategically significant growth zones. These areas may require targeted infrastructure enhancements to address future energy demand effectively and support anticipated development.

Additionally, the energy distribution pattern suggests horizontal growth in specific segments, aligning with historical expansion trends documented by the distribution company. Furthermore, the use of the 9 × 9 core matrix demonstrates its capability to accurately predict long-term energy consumption patterns, including the identification of two (02) new areas in segment S1 over the 20-year horizon. This result is consistent with the historical horizontal growth observed by the distribution company, emphasizing the reliability and robustness of the proposed forecasting approach in accommodating dynamic urban expansion and evolving consumption trends.

Table 16. Spatial forecast for the year 2043 in S1—9 × 9 matrix (GWh).

Y↓/X→	27	28	29	30	31	32	33	34	35	36
871							21.3			
870						2.1	21.0		9.8	
869						3.8	28.0	8.7	8.4	
868			55.5		79.5	32.6	46.5	28.2		
867		168.8	1088.8	364.6	74.2		43.4			
866	1158.2	3607.7	549.4	102.1						
865	401.9	2582.2	653.5	41.4						
864		489.0	1296.4	417.6	**16.1**					
863			45.5	264.4						
862				48.7	45.9					
861				66.4	340.3	49.7	45.5			
860					52.4	83.4				
859						211.5				
858						38.1	44.1			
857							**17.3**			
					14,754.2					

Finally, Figure 12 shows the geospatial forecasting results for the year 2043, depicted in red. Figure 12a, 12b, and 12c correspond to segments S1, S2, and S3, respectively. These results were obtained using the 9 × 9 convolutional kernel.

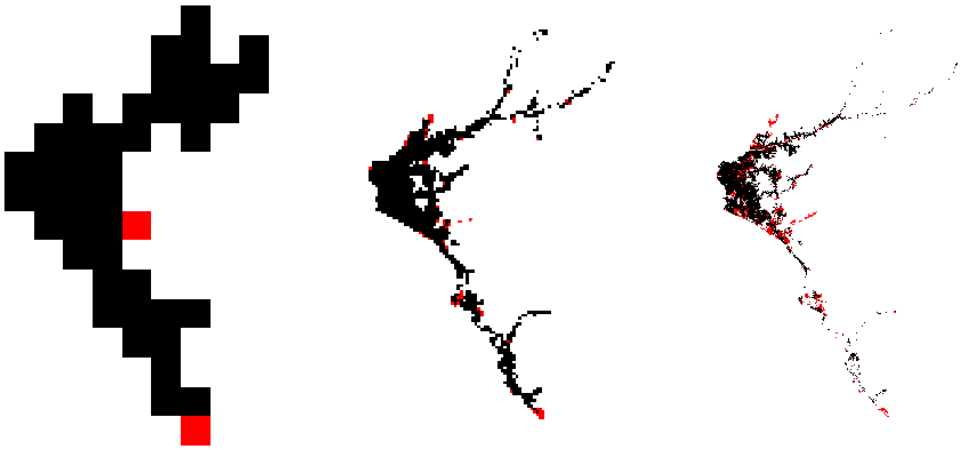

(**a**) (**b**) (**c**)

Figure 12. Geospatial forecast for the year 2043: kernel 9 × 9. (**a**): Segment S1; (**b**): segment S2; (**c**): segment S3.

6. Conclusions

The proposed geospatial analysis algorithm demonstrates remarkable versatility and efficacy in addressing both system-wide energy forecasting and segmented consumption analysis. By integrating relative growth trends across consumption areas of varying scales, the algorithm enables precise modeling and strategic planning. Its ability to incorporate new consumption zones, constrained only by geographic limitations, ensures adaptability to dynamic urban expansion and evolving development needs.

In the evaluated case study, which utilized 17 years of historical data (11 years for training and 6 years for validation), the 9 × 9 core matrix exhibited superior performance for segments with scales of 1:10,000 and 1:1000. For smaller-scale segments at a 1:100 ratio, higher-order core matrices yielded better results. However, due to the smaller scale and inherent historical distortions in consumption patterns, additional data would be required to enhance accuracy in long-term forecasting for these cases.

The proposed methodology, along with the developed algorithms for consumption segmentation, learning models, and convolution operations, is fully implementable by electrical distribution companies, even those with limited historical records. Moreover, for the analyzed distribution system, the proposed geospatial energy consumption forecasting model extends over a 20-year horizon, offering a practical and scalable solution for long-term planning and system optimization.

7. Recommendations

The proposed model's primary limitation is the dynamic nature of coverage factors, which require greater precision for smaller-scale grids (e.g., 100 m resolution). To enhance long-term geospatial forecasting, geographic systems and cadastral data must be periodically updated.

Incorporating additional spatial analysis parameters, such as physical or economic proximity factors, can further refine forecasting models. Growth patterns from logistic and Gompertz curves (S-curves) could also be integrated at various scales using optimization or machine learning techniques.

The analysis of satellite images to detect night lights offers potential applications, in particular for assessing demand in areas without an electricity grid. These data can be incorporated into the proposed algorithm as an additional parameter and guide the location of new "isolated" grids in the forecast and their integration into the existing electricity grid.

Incorporating real-time data from IoT sensors can significantly enhance geospatial demand analysis. Data such as electricity consumption, solar resources, wind resources, temperature, and other environmental factors can make spatial analyses more dynamic and responsive.

For more heterogeneous or larger-scale datasets, it is recommended to evaluate the suitability of alternative methods, such as DBSCAN and GMM for clustering, as well as models like LSTMs to determine relative growth. Defining the number of segments, grid sizes, and convolutional kernel is essential to ensure the effectiveness of the proposed methodology.

The proposed methodology can also be applied to other essential services such as gas and water. However, adaptations are necessary to accommodate different types of data and the specific dynamics of each resource. These modifications are crucial to achieve effective integration into the planning of multi-energy systems.

Include the analysis of the demand characterization factors for the geospatial forecast of the maximum demand in the different components of the electrical infrastructure. This analysis can be addressed using machine learning techniques (load factor) and the Monte Carlo method (simultaneity factor).

Author Contributions: Conceptualization, H.C. and Y.M.; methodology, H.C. and Y.M.; validation, H.C. and Y.M.; investigation, H.C. and Y.M.; writing—review and editing, H.C. and Y.M.; visualization, H.C. and Y.M.; supervision, Y.M. All authors have read and agreed to the published version of the manuscript.

Funding: This research was funded by the National Council for Scientific and Technological Development (CNPq) under Grant No. 03/2021 and Process No. 304779/2021-0.

Data Availability Statement: The original contributions presented in the study are included in the article, further inquiries can be directed to the corresponding author.

Acknowledgments: The authors gratefully acknowledge the invaluable support provided by the Faculty of Mechanical Engineering at the National University of Engineering, Lima, Peru, and the Department of Electrical Engineering at the Federal University of Paraíba, Brazil.

Conflicts of Interest: The authors declare no conflict of interest.

References

1. Hammad, M.A.; Jereb, B.; Rosi, B.; Dragan, D. Methods and Models for Electric Load Forecasting: A Comprehensive Review. *Logist. Supply Chain. Sustain. Glob. Chall.* **2020**, *11*, 51–76. [CrossRef]
2. Panda, S.K.; Jagadev, A.K.; Mohanty, S.N. Forecasting Methods in Electric Power Sector. *Int. J. Energy Optim. Eng. (IJEOE)* **2018**, *7*, 1–21. [CrossRef]
3. Singh, A.K.; Ibraheem; Khatoon, S.; Muazzam, M.; Chaturvedi, D.K. Load forecasting techniques and methodologies: A review. In Proceedings of the 2012 2nd International Conference on Power, Control and Embedded Systems, Allahabad, India, 17–19 December 2012; pp. 1–10. [CrossRef]
4. Klyuev, R.V.; Morgoev, I.D.; Morgoeva, A.D.; Gavrina, O.A.; Martyushev, N.V.; Efremenkov, E.A.; Mengxu, Q. Methods of Forecasting Electric Energy Consumption: A Literature Review. *Energies* **2022**, *15*, 8919. [CrossRef]
5. Dashti, R.; Rouhandeh, M. Power distribution system planning framework (A comprehensive review). *Energy Strategy Rev.* **2023**, *50*, 101256. [CrossRef]
6. Li, Q.; Yang, L.; Huang, S.; Liu, Y.; Guo, C. The Effects of Urban Sprawl on Electricity Consumption: Empirical Evidence from 283 Prefecture-Level Cities in China. *Land* **2023**, *12*, 1609. [CrossRef]
7. Kuster, C.; Rezgui, Y.; Mourshed, M. Electrical load forecasting models: A critical systematic review. *Sustain. Cities Soc.* **2017**, *35*, 257–270. [CrossRef]
8. Ahmad, N.; Ghadi, Y.; Adnan, M.; Ali, M. Load Forecasting Techniques for Power System: Research Challenges and Survey. *IEEE Access* **2022**, *10*, 71054–71090. [CrossRef]
9. Mystakidis, A.; Koukaras, P.; Tsalikidis, N.; Ioannidis, D.; Tjortjis, C. Energy Forecasting: A Comprehensive Review of Techniques and Technologies. *Energies* **2024**, *17*, 1662. [CrossRef]

10. Habbak, H.; Mahmoud, M.; Metwally, K.; Fouda, M.M.; Ibrahem, M.I. Load Forecasting Techniques and Their Applications in Smart Grids. *Energies* **2023**, *16*, 1480. [CrossRef]
11. Verwiebe, P.A.; Seim, S.; Burges, S.; Schulz, L.; Müller-Kirchenbauer, J. Modeling Energy Demand—A Systematic Literature Review. *Energies* **2021**, *14*, 7859. [CrossRef]
12. Kumar, R. A Comprehensive Study on Demand Forecasting Methods and Algorithms for Retail Industries. *J. Univ. Shanghai Sci. Technol.* **2021**, *23*, 409–420.
13. Blagajac, S.; Krajcar, S.; Skrlec, D. A computational tool to support spatial electric load forecasting. In Proceedings of the 2000 10th Mediterranean Electrotechnical Conference. Information Technology and Electrotechnology for the Mediterranean Countries. Proceedings. MeleCon 2000 (Cat. No.00CH37099), Lemesos, Cyprus, 29–31 May 2000; Volume 3, pp. 1116–1119. [CrossRef]
14. Ying, L.C.; Pan, M.C. Using adaptive network based fuzzy inference system to forecast regional electricity loads. *Energy Convers. Manag.* **2008**, *49*, 205–211. [CrossRef]
15. Carreno, E.M.; Rocha, R.M.; Padilha-Feltrin, A. A Cellular Automaton Approach to Spatial Electric Load Forecasting. *IEEE Trans. Power Syst.* **2011**, *26*, 532–540. [CrossRef]
16. Melo, J.D.; Carreno, E.M.; Padilha-Feltrin, A. Spatial load forecasting using a demand propagation approach. In Proceedings of the 2010 IEEE/PES Transmission and Distribution Conference and Exposition: Latin America (TD-LA), Sao Paulo, Brazil, 8–10 November 2010; pp. 196–203. [CrossRef]
17. Melo, J.D.; Carreno, E.M.; Padilha-Feltrin, A. Multi-agent framework for spatial load forecasting. In Proceedings of the 2011 IEEE Power and Energy Society General Meeting, Detroit, MI, USA, 24–29 July 2011; pp. 1–8. [CrossRef]
18. Melo, J.D.; Carreno, E.M.; Padilha-Feltrin, A. Considering Urban Dynamics in spatial electric load forecasting. In Proceedings of the 2012 IEEE Power and Energy Society General Meeting, San Diego, CA, USA, 22–26 July 2012; pp. 1–7. [CrossRef]
19. Xiao, B.; Guo, P.; Mu, G.; Yan, G.; Li, P.; Cheng, H.; Li, J.; Bai, Y. A Spatial Load Forecasting Method Based on the Theory of Clustering Analysis. *Phys. Procedia* **2012**, *24*, 176–183. [CrossRef]
20. Jain, R.K.; Smith, K.M.; Culligan, P.J.; Taylor, J.E. Forecasting energy consumption of multi-family residential buildings using support vector regression: Investigating the impact of temporal and spatial monitoring granularity on performance accuracy. *Appl. Energy* **2014**, *123*, 168–178. [CrossRef]
21. Shin, J.H.; Yi, B.J.; Kim, Y.I.; Lee, H.G.; Ryu, K.H. Spatiotemporal Load-Analysis Model for Electric Power Distribution Facilities Using Consumer Meter-Reading Data. *IEEE Trans. Power Deliv.* **2011**, *26*, 736–743. [CrossRef]
22. Wu, H.C.; Lu, C.N. A Data Mining Approach for Spatial Modeling in Small Area Load Forecast. *IEEE Power Eng. Rev.* **2002**, *22*, 60. [CrossRef]
23. Wu, J.; He, S.; Yang, Y. Application of Particularity Decision Method in Spatial Load Forecasting. In Proceedings of the 2010 Second WRI Global Congress on Intelligent Systems, Wuhan, China, 16–17 December 2010; Volume 2, pp. 173–176. [CrossRef]
24. Vasquez-Arnez, R.L.; Jardini, J.A.; Casolari, R.; Magrini, L.C.; Semolini, R.; Pascon, J.R. A methodology for electrical energy forecast and its spatial allocation over developing boroughs. In Proceedings of the 2008 IEEE PES Transmission and Distribution Conference and Exposition, Chicago, IL, USA, 21–24 April 2008; pp. 1–6. [CrossRef]
25. Willis, H.L. *Power Distribution Planning Reference Book*, 2nd ed.; CRC Press: Boca Raton, FL, USA, 2004. [CrossRef]
26. Willis, H.L. *Spatial Electric Load Forecasting*, 2nd ed.; CRC Press: Boca Raton, FL, USA, 2002. [CrossRef]
27. Vieira, D.; Silva, B.; Menezes, T.; Lisboa, A. Large scale spatial electric load forecasting framework based on spatial convolution. *Int. J. Electr. Power Energy Syst.* **2020**, *117*, 105582. [CrossRef]
28. Liu, Z.; Pan, W.; Liu, J.; Wen, K.; Gong, J. A combined approach for forecasting regional long-term natural gas demand integrating K-means clustering, grey theory, and BP neural network. *Oil Gas Storage Transp.* **2024**, 103–110.